DOI: 10.1002/cplu.201200039

Polypyridyl Complexes of Ruthenium(II): Stabilization of G-quadruplex DNA and Inhibition of Telomerase Activity

Du Liu,[a] Yanan Liu,[a] Chuan Wang,[a] Shuo Shi,[c] Dongdong Sun,[a] Feng Gao,*[b] Qianling Zhang,*[d] and Jie Liu*[a]

Two ruthenium(II) complexes $[Ru(phen)_2(tip)](ClO_4)_2$ (**1**) and $[Ru(bpy)_2(tip)](ClO_4)_2$ (**2**; phen = 1,10-phenanthroline, bpy = 2,2′-bipyridine, tip = 2-thiophenimidazo[4,5-*f*][1,10]phenanthroline) were synthesized and characterized by elemental analysis, ^{1}H NMR spectroscopy, and electrospray ionization-mass spectrometry to explore the role of metal complexes as novel telomeric quadruplex stabilizers. The different quadruplex binding properties of these compounds were evaluated by absorption and emission analyses, circular dichroism spectroscopy, fluorescence resonance energy transfer (FRET) melting assay, NMR spectroscopy, and molecular modeling. The results show that both complexes can well induce and stabilize different G-quadruplex structures using a 1:1 [quadruplex]/[complex] binding mode ratio. Complex **1** exhibits higher interaction ability at 1.43×10^6 M^{-1} binding affinity and superior G-quadruplex selectivity over duplex DNA through multiple interaction (mainly intercalating) with the G-quadruplex at the 3′-terminal face. Furthermore, polymerase chain reaction (PCR)-stop assay, electrophoretic mobility shift assay, telomerase repeat amplification protocol, and MTT assay demonstrate that complex **1** not only can stabilize dimer forms of the G-quadruplex at low concentrations but also exhibit better inhibitory activity for telomerase and cancer cells. The results suggest that complex **1** may be a potential telomerase inhibitor for cancer chemotherapy.

Introduction

G-quadruplexes (or G-tetrads) are functionally useful secondary DNA structures containing G-quartets stabilized through Hoogsteen hydrogen bonding.[1] These structures are found throughout the human genome and are currently being considered as potential anticancer targets.[2] Telomeric DNA consists of tandem repeats of sequence d[(TTAGGG)*n*] and is the most studied DNA sequence. This sequence can cap the ends of chromosomes and protect them from deleterious processes during replication steps.[3] A previous study has indicated that telomeric DNA may fold into G-quadruplex structures in the presence of metal ions, such as K^+ or Na^+.[4] The formation of G-quadruplex by telomeric DNA inhibits the activity of telomerase,[5] an enzyme not found in most normal somatic cells, but present in 85–90% of cancer cells and contributes to the immortality of these cells.[6] Therefore, the design of drugs that target and stabilize the telomeric G-quadruplex is a rational and promising approach to interfere with telomerase activity in tumor cells and to act as potential anticancer agents.[7]

Recently, several research groups have synthesized a number of small-molecule ligands for G-quadruplex structure stabilization and telomerase activity inhibition.[8] Several metal complexes, which generally have a positively charged center or substituents and π-delocalized system, have been reported to interact with G-quadruplex.[9]

Octahedral metal complexes can also be designed to bind G-quadruplex using a large planar aromatic intercalating ligand for DNA binding and ancillary ligands for shape and functional group recognition within the major groove.[10]

Ruthenium(II) complexes with polypyridyl ligands as typical octahedral metal complexes have prominent DNA binding properties resulting from a combination of easily constructed rigid chiral structures spanning all three spatial dimensions and a rich photophysical repertoire.[11] Some of these complexes have been investigated as nucleic acid probes, synthetic restriction enzymes, anticancer drugs, and DNA footprinting agents, among others.[12] To date, a few Ru^{II} complexes have been found to promote the formation and stabilization of G-quadruplexes.[13] Shi et al. have reported the remarkable ability of a novel dinuclear complex to promote an antiparallel G-quadruplex formation.[14] Ruthenium(II) complexes containing the dppz ligand can serve as a prominent molecular "light switch" for both G-quadruplexes and i-motif, but it preferentially binds to G-quadruplexes over the i-motif.[15] Thomas and co-workers investigated the binding preferences of a dinuclear

[a] *Dr. D. Liu,[+] Y. Liu,[+] C. Wang, D. Sun, Prof. J. Liu*
Department of Chemistry, Jinan University
Guangzhou 510632 (P. R. China)
Fax: (+86) 20-8522-1263
E-mail: tliuliu@jnu.edu.cn

[b] *Dr. F. Gao*
School of Chemistry and Chemical Engineering, Sun Yat-Sen University
Guangzhou 510275 (P. R. China)

[c] *Prof. S. Shi*
Department of Chemistry, Tongji University
Shanghai 200092 (P. R. China)

[d] *Prof. Q. Zhang*
Chemistry and Chemical Engineering, Shenzhen University
Shenzhen 518061 (P. R. China)

[+] *These authors contributed equally to this work.*

Supporting information for this article is available on the WWW under http://dx.doi.org/10.1002/cplu.201200039.

ruthenium(II) complexes with different quadruplex DNA structures. It was found that the differences in quadruplex binding affinity and optical signature are rationalized through a consideration of the structural features of the quadruplexes.[16] In 2011, they found that polypyridyl complexes of Ru^{II} display sequence selectivity and high-affinity binding to duplex DNA through groove binding.[17] However, they have not determined whether the inhibition of telomerase activity is relevant to the stabilization of this G-quadruplex, or even if there are further effects of the antitumor activity.

Herein, two Ru^{II} complexes $[Ru(phen)_2(tip)](ClO_4)_2$ (**1**) and $[Ru(bpy)_2(tip)](ClO_4)_2$ (**2**; phen = 1,10-phenanthroline, bpy = 2,2′-bipyridine, tip = 2-thiophenimidazo[4,5-*f*][1,10]phenanthroline), which show some interesting properties through interaction with G-quadruplex DNA, were designed and synthesized. The spectroscopic, biochemical, and cellular properties of these compounds were examined to reveal their interactions with the telomeric G-quadruplex DNA (HTG21) as well as the relationship between the inhibition of telomerase and antitumor activities. The title complexes acting as G-quadruplex stabilizers showed effective inhibition of telomerase and antitumor activities, thus suggesting that telomerase G-quadruplex may act as a potential antitumor agent. The synthetic route and structure of complex **1** and **2** are shown in Scheme 1.

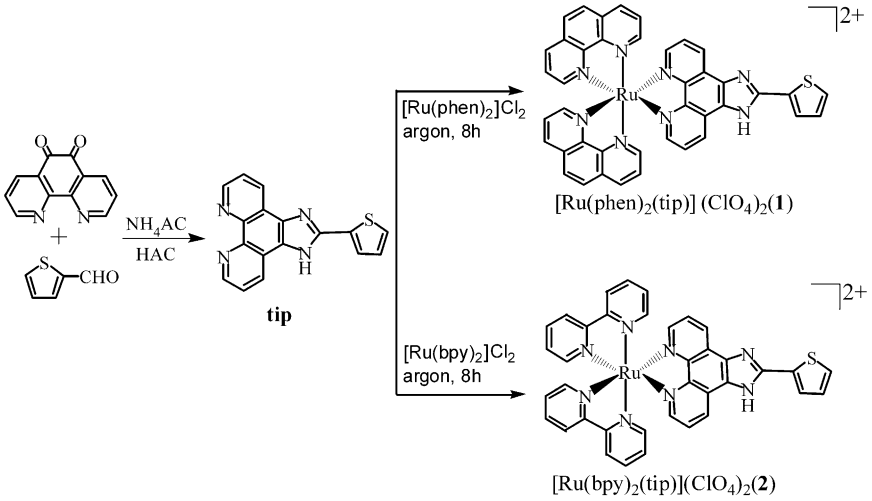

Scheme 1. Synthetic routes for the ligand (**tip**) and ruthenium complexes $[Ru(phen)_2(tip)](ClO_4)_2$ (**1**) and $[Ru(bpy)_2(tip)](ClO_4)_2$ (**2**). HAC = CH_3COOH.

Results and Discussion

Fluorescence behavior of G-quadruplex and duplex DNA (ds26)

Zhou and co-workers have reported fluorescence selectivity as an approach to detect the selectivity between G-quadruplex and other DNA structures.[18] Here, the fluorescence behavior of Ru complexes with different DNA is reported. Human telomeric DNA (HTG21) was selected to form the G-quadruplex structures in the presence of K^+, whereas ds26 was selected as the duplex DNA structure. The results of the different fluorescence spectra are shown in Figure 1. Both complexes **1** and **2** emit luminescence at ambient temperature, with a maximum appearing at 598 nm.

Upon the addition of different DNA, it was clear that there was a more remarkable fluorescence enhancement in the presence of HTG21 than ds26. This observation maybe implies that the complexes are more inaccessible to water molecules and that there is a greater overlap between the aromatic surfaces of the metal complexes and the bases when bound to quadruplex as opposed to duplex DNA.[16,19] In particular, complex **1**

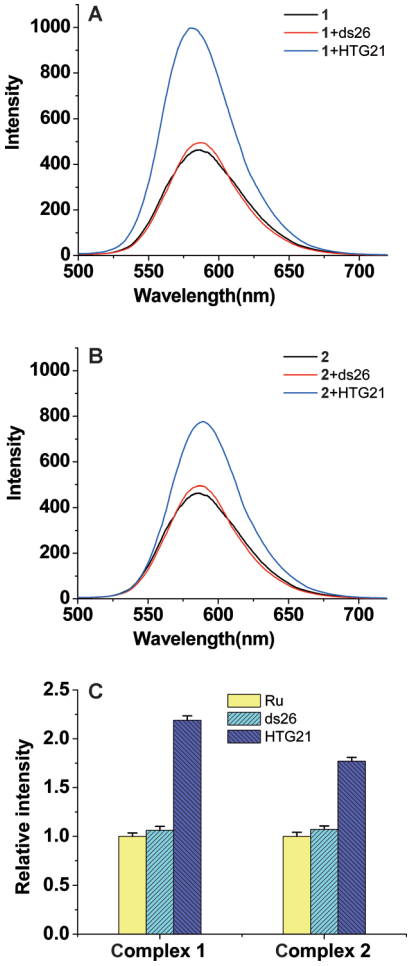

Figure 1. Emission comparison of 5 μM solution of complexes **1** (A) and **2** (B) in the presence of HTG21 and ds26 using Tris-KCl buffer (100 mM KCl, 10 mM Tris-HCl, pH 7.4, [Ru]/[DNA] = 2:1) at λ_{ex} = 460 nm. C) Relative fluorescence strength of complexes **1** and **2**. Results are the mean values of at least three independent experiments.

promoted a bigger fluorescence intensity of the G-quadruplex, more than 1.2 times larger than duplex DNA, whereas complex **2** only has 0.7-fold increase in selectivity for G-quadruplex. The different fluorescence behaviors between the two Ru^{II} complexes and telomeric quadruplex inspired us to further study their different DNA-binding properties by a variety of research methods.

Emission spectra analyses and binding affinities

Given that fluorescence spectra can reflect the information about the local environmental changes in a chromophore, then these spectra can be used to probe the interaction between the fluorophore and its environment.[20] In the current experiment, the binding of the Ru complexes to G-quadruplex DNA (HTG21) was investigated using fluorescence titration. The results are illustrated in Figure 2. Upon the addition of

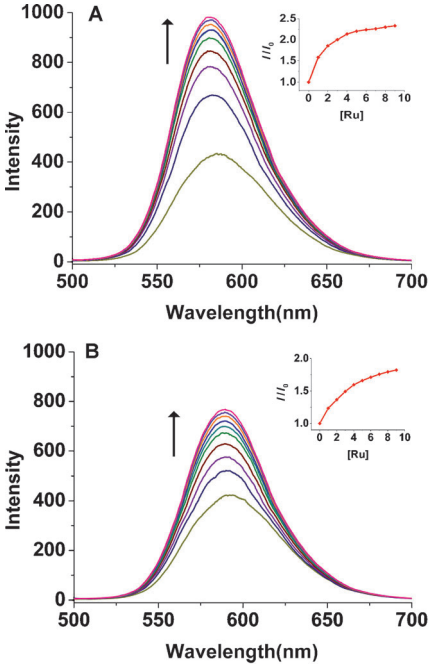

Figure 2. Emission spectral traces of complexes **1** (A) and **2** (B) in Tris-KCl buffer (100 mM KCl, 10 mM Tris-HCl, pH 7.4) at increasing ratios of [HTG21]/[Ru] = 0–2.0, [Ru] = 5 μM.

HTG21, the emission intensities of complexes **1** and **2** increased to approximately 1.32 and 0.8 times larger than the original intensities, respectively. The enhanced fluorescence in these complexes implies that these complexes can interact with HTG21 and be protected by DNA efficiently, because the hydrophobic environment inside the DNA helix decreases the accessibility of solvent water molecules to the complex and thus the complex mobility is restricted at the binding site, thus leading to the decrease of vibrational modes of relaxation.[17,21] Based on the emission enhancement, the intrinsic binding constant was obtained according to the Scatchard Equation (1):

$$r/C_f = nK_b - rK_b \quad (1)$$

$$r = C_b/C_{DNA}$$

$$C_b = C_t \cdot (F - F_0)/(F_{max} - F_0)$$

where C_t is the total compound concentration, F is the observed fluorescence emission intensity at given DNA concentration, F_0 is the intensity in the absence of DNA, and F_{max} is the fluorescence of the totally bound compound. Binding data were cast into the form of a Scatchard plot of r/C_f versus r, where r is the binding ratio $C_b/[DNA]$, and C_f is the free ligand concentration.[22] The values of the binding constants for complexes **1** and **2** with G-quadruplexes were 1.43×10^6 and $6.33 \times 10^5\ M^{-1}$, respectively. These observations imply that the interaction between complex **1** and quadruplex DNA is stronger compared with that between complex **2** and the quadruplex DNA.

Absorption spectroscopy studies and binding ability

Electronic spectra of the complexes in the absence and presence of quadruplex were obtained to gain insight into the binding ability between the Ru^{II} complexes and G-quadruplex DNA (Figure S1 in the Supporting Information). Both Ru^{II} complexes were characterized using a metal-to-ligand-charge-transfer (MLCT) transition band and an intraligand (IL) absorption band at approximately 457 and 288 nm, respectively. However, another narrow separated band at approximately 263 nm was present in complex **1**. Upon the addition of HTG21, both the MLCT and IL absorption bands of these Ru^{II} complexes exhibited obvious hypochromisms (H) and red shifts ($\Delta\lambda$), thus indicating that both complexes can intercalate the G-quadruplex.[23]

The addition of HTG21 to the solution of complex **1** led to a red shift of 6 nm at 457 nm and hypochromism of 25.1% for the band at 288 nm. However, the addition of HTG21 to the solution of complex **2** in the same buffer led to only a red shift of 3 nm and 11.1% hypochromism of the band at 457 nm (Table 1). The absorption titration is well consistent with the result of the emission spectroscopic analysis. The higher binding affinity of complex **1** is probably results from the greater planar area of the ancillary ligand, intercalating with the base pairs or entering into the grooves within DNA.[17,24]

Table 1. Absorption spectra (λ_{max}) and DNA-binding date of complexes **1** and **2**.

Complex	λ_{max} (free) [nm]	λ_{max} (bound) [nm]	$\Delta\lambda$ [nm]	ΔH [%]
1	263	264	1	24.8
	288	290	2	25.1
	457	463	6	11.8
2	288	289	1	19.2
	457	460	3	11.1

Continuous variation analysis and binding stoichiometric ratios

Continuous variation analysis using the luminescence intensities was performed to further validate the meaningful binding stoichiometries of the Ru complexes with quadruplex DNA (Figure 3). The point of intersection for complexes **1** and **2** with telomeric G-quadruplex is $X = 0.51$ and 0.56, respectively. These data are consistent with the 1:1 [quadruplex]/[complex] binding mode, suggesting a specific ruthenium–quadruplex interaction with a single guanine tetrad.[25]

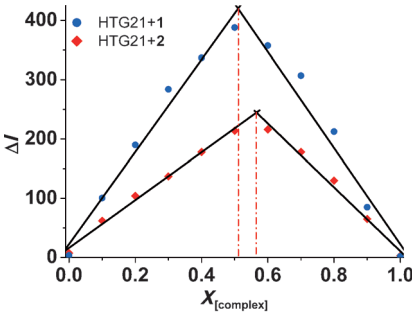

Figure 3. The result of continuous variation analysis for complexes **1** and **2** with HTG21 in Tris-KCl buffer (100 mM KCl, 10 mM Tris-HCl, pH 7.4).

Stability of G-quadruplex by the fluorescence resonance energy transfer (FRET) melting assay

Thermodynamic stability of the Ru complexes to G-quadruplex DNA was determined using the melting temperature of the G-quadruplex DNA by a FRET melting assay. Change in melting temperature (ΔT_m) values were calculated by subtracting the T_m of the nucleic acid with the complex from the T_m of the free fluorescent-labeled oligonucleotide F21T. The ΔT_m values of the F21T DNA treated with the complexes are calculated, and their concentration-dependent melting curves are shown in Figure 4A,B. All T_m values of the samples incubated with the complexes increased compared with the control value (51.5 °C), thus indicating that the Ru complexes could enhance the thermodynamic stability of this oligomer. The 12.8 °C increase in the melting temperature (ΔT_m) of complex **1** at [Ru]/[F21T] = 10 ratio shows its high degree of stabilization for G-quadruplex DNA. Hence, complex **1** is a more effective stabilizer of G-quadruplex DNA than complex **2** ($\Delta T_m = 8.8$ °C). These activity differences are in accordance with the result of the above studies.

Thermal denaturation analyses by circular dichroism (CD) spectroscopy were also conducted to determine further the complex-induced stabilization of a folded quadruplex. As the ratio of Ru complexes to HTG21 equaled 10 (i.e. [HTG21] = 2 μM, [Ru] = 20 μM), thermal denaturation curves from the CD signal at 295 nm are shown in Figure 4C. Complex **2** has a weak stabilizing effect on G-quadruplex, with only approximately 8.6 °C increase in the T_m value, whereas complex **1** could increase the T_m value from 60.2 to 73.4 °C (Table S1). This result is consistent with the FRET assay results, further implying that complex **1** possesses a higher stabilizing ability than complex **2**.

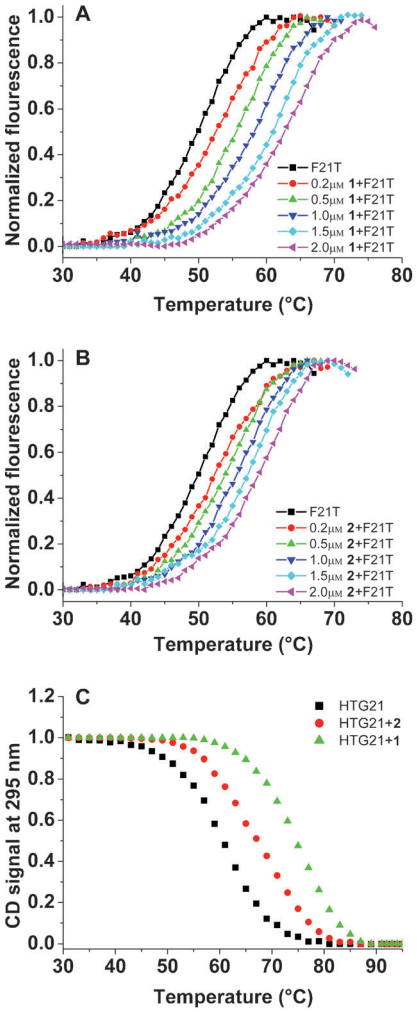

Figure 4. Plot of ΔT_m versus complex concentrations. FRET melting profiles of 0.2 μM F21T with complexes **1** (A) and **2** (B) in Tris-KCl buffer. C) Thermal denaturation curves from a CD signal at 295 nm with 2 μM HTG21 and in the presence of complexes **1** and **2** (20 μM) in Tris-KCl buffer.

Furthermore, the G-quadruplex selectivity of complexes was assessed by a competition FRET experiment where different ratios of nonfluorescent duplex DNA (ds26) were added to the classic FRET experiment with the telomeric sequence F21T (Figure 5).[26] In the presence of various amounts of competitor ds26, the thermal stabilization of F21T enhanced by the complexes was slightly affected, whereas the addition of a 50× molar excess of base pairs induces a decrease in stabilization (Figure 5C).[27] The results suggest that the binding of Ru complexes to a quadruplex is at least 40-fold higher than that to a duplex. The combined results of FRET competition assay, which well verifies the fluorescence selectivity, demonstrate that the title complexes can be considered as a new class of highly selective G-quadruplex binding ligands.

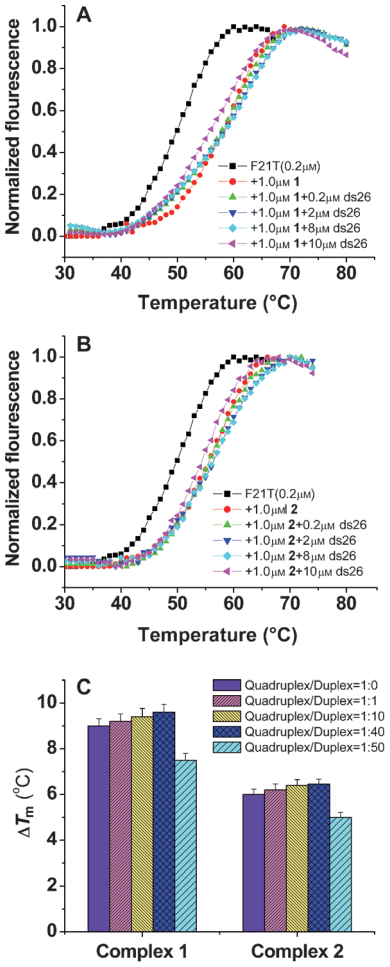

Figure 5. Competitive FRET melting curves of F21T with 1 μM of complexes **1** (A) and **2** (B) and duplex competitor ds26 in Tris-KCl (100 mM KCl, 10 mM Tris-HCl, pH 7.4) F21T = 0.2 μM. C) Competition FRET experiment of complexes for the G-quadruplex DNA sequence over duplex DNA. Results are the mean values of at least three independent experiments.

Nuclear magnetic resonance (NMR) spectroscopy analysis and binding sites

Nuclear magnetic resonance titration experiments were conducted to understand the binding sites of the interaction with the G-quadruplex structures. Complex **1** was added into a G4 A3-quadruplex prepared from a shorter oligonucleotide as telomere sequence (G4 A3: 5′-TAGGGTTA-3′).[28] The numbering of the residues, starting at the 5′ end of the DNA sequence, is T1, A2, G3, G4, G5, T6, T7, and A8. The imino group resonances of G3, G4, and G5 were at $\delta = 11.5$, 11.3, and 10.8 ppm, respectively (Figure 6), and are in agreement with a previous report.[29] Upon the titration of complex **1**, the proton signal corresponding to the G5-imino unit first exhibited broadening compared with the others, thus suggesting that complex **1** first binds close to the 3′-terminal face of the G-quadruplex DNA. At a [**1**]/[G4 A3-quadruplex] ratio of 0.5, all the imino resonances at $\delta = 10.8$–12 ppm experienced significant broadening consistent with the multiple stacking configurations on the top of the G-tetrad. Such differential broadening are nearly

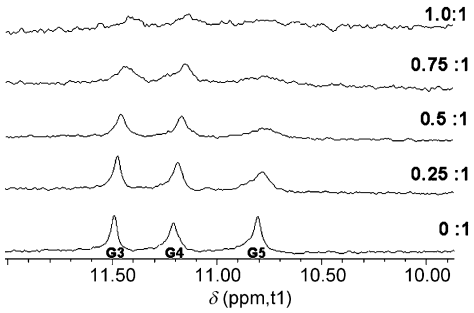

Figure 6. ^{1}H NMR analysis of titration of the G4 A3-quadruplex with complex **1** at various [Ru]/[G4 A3-quadruplex] ratios in 90% H_2O/10% D_2O with 150 mM KCl, 25 mM KH_2PO_4, 1 mM EDTA (pH 7.40). Only the proton signals corresponding to the imino group (400 MHz, 25 °C) are shown.

identical to those exhibited by [Pt^{II}(dppz-COOH)(NC)]CF_3SO_3 (dppz-COOH = 11-carboxydipyrido[3,2-*a*:2′,3′-*c*]phenazine)[28] and Hoechst 33258,[30] both of which are known to bind to a G-quadruplex. Combined with the optical experiments and the NMR analysis, we predict that complex **1** prefers intercalating with the G-tetrad at 3′-terminal face and/or multiple stacking on the G-tetrad.

Molecular modeling and binding mode

To provide insight into the binding mode(s), four different binding sites of **1** with intermolecular G-quadruplex d(T_2AG_3T)$_4$ (PDB code 1NP9) were investigated by molecular modeling studies. For this calculation by software, every possible binding angle (0–360°, including both major and minor grooves), surrounding the axis of quadruplex has been estimated, and the results shown in Figure 7 are geometries with the lowest energy among all these possible binding modes between each adjacent G4 planes. The estimated interaction energy changes for each model are shown in Table 2. It was found that when

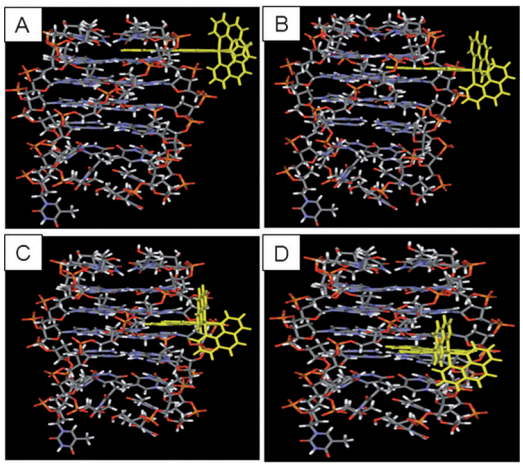

Figure 7. Energy-minimized structures for possible binding sites of the complex **1** with (A) 5′-TAGGG*TTA-3′, (B) 5′-TAGG*GTTA-3′, (C) 5′-TAG*GGTTA-3′, and (D) 5′-TA*GGGTTA-3′, where the asterisks represent binding sites. The Ru^{II} complex is shown in yellow.

Table 2. Estimated interaction energy (ΔE) of possible binding sites of complex **1** with $d(T_2AG_3T)_4$ by molecular modeling studies.

Binding sites	ΔE [kcal mol^{-1}]
5′-TAGGG*TTA-3′	−52.2
5′-TAGG*GTTA-3′	−43.6
5′-TAG*GGTTA-3′	−46.3
5′-TA*GGGTTA-3′	−44.7

the planar ligand intercalates into the G-quadruplex, the square π-aromatic plane stacks on the 3′-terminal G-tetrads (Figure 7A), exhibiting a smaller binding energy (−52.20 kcal mol^{-1}) than the other three possible binding models (Figure 7B,D). This notable result indicates that **1** preferred intercalating into the exterior 3′ surface of G-quadruplex with 1:1 stoichiometry, which is consistent with the model derived from the results of continuous variation analysis and NMR experiments, as described in the previous section. Notably, more energy will be required to intercalate into the G-quadruplex more effectively for the whole complex. This result validates the hypothesis that it is difficult for the octahedral metal complex itself to be embedded in a π-stacking unit or even in direct proximity to the G-tetrads, but the charged molecule as a whole interacts with grooves/loops and the phosphate backbone of quadruplexes.[31] In view of the most favorable biding mode (Figure 7A), we can figure out that 1,10-phenanthroline, as a larger planar ancillary ligand, provides more possibilities to interact with grooves/loops and the phosphate backbone of quadruplexes in addition to the intercalative interaction and/or multiple stacking on the G-tetrad binding. Such results may explain why complex **1**, with the same positively charged center as in complex **2**, is a more efficient G-quadruplex binder.

Inducing/stabilizing the G-quadruplex structure by circular dichroism (CD) spectroscopy

The G-rich telomeric sequence forms intra- and intermolecular G-quadruplexes in monomeric (M), dimeric (D), and tetrameric (T) structures through multiple methods (Scheme 2).[32] Circular dichroism spectroscopy is one of the well-established methods for determining the presence and to some degree the folding of G-quadruplex structures. All guanine units in the parallel-stranded G-quadruplex have the same *anti* glycosidic conformation, exhibiting a large positive band at 295 nm and a negative band at 240 nm.[33] By contrast, guanine units in the antiparallel-stranded G-quadruplex have alternating *anti* and *syn* glycosidic conformations along each DNA strand, exhibiting a characteristic positive band at 295 nm, a smaller negative band at 265 nm, and a smaller positive band at 245 nm in the CD spectra.[34] Here, complex binding studies were conducted in the absence and presence of a stabilizing salt by CD spectroscopy to investigate the induction and conversion among various kinds of human telomeric quadruplexes. In addition, to measure the real CD signal, we deducted background noise of complexes (Figure S2) and the results in Figure 8 and Figure S3 show just the CD signal from the HTG21.

In the absence of any salt, the HTG21 oligonucleotide was dissociated partially to single-stranded molecules with a negative band centered at 238 nm, a major positive band at 257 nm, a minor negative band at 280 nm, and a positive band near 295 nm (Figure 8A,B, black line). The bands at 238 and 257 nm disappeared gradually upon the addition of complex **2** (0–12 μM), thereby revealing a major negative band at 260 nm and significantly increasing the intensity of the band centered at 295 nm (Figure 8B). These changes are consistent with the induction of the guanine-rich DNA in forming the antiparallel G-quadruplex structure by complex **2**. Aside from the similar changes as for the addition of complex **2**, a new and positive band at 270 nm was observed in the CD signal upon the addition of complex **1** to the same solution (Figure 8A). This result indicates that complex **1** can induce HTG21 to form a hybrid-type quadruplex. In addition, this striking trait suggests that the binding of the Ru complexes to DNA causes their remarkable ability to promote different quadruplex formations (Figure 8C).

Furthermore, CD experiments were conducted in a solution of Na^+ or K^+ ions to determine whether the compounds could lead to structural conversion. Figure 9A,B show that the quadruplex molecules exist as typical parallel G-quadruplexes conformations in the presence of K^+, revealing a large positive band at 295 nm and a negative band at 240 nm.[33] Although no significant change was found, the intensity of CD signals corresponding to DNA was altered after the addition of complex **2** to HTG21. However, the intensity of the negative band at 260 nm increased significantly with an increasing amount of

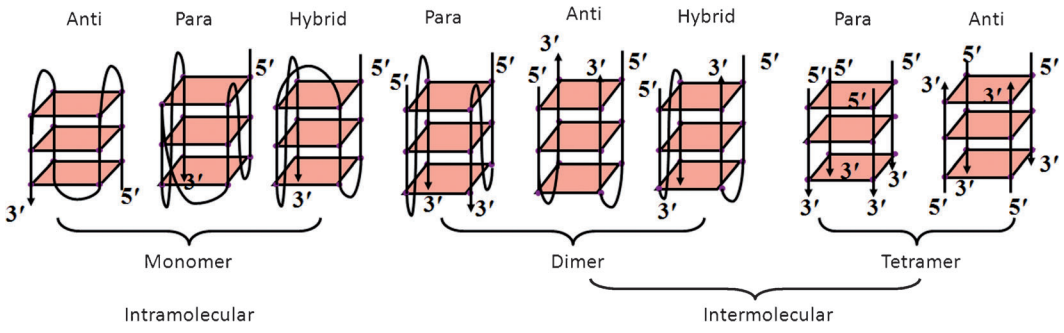

Scheme 2. Schematic representation of the G-quadruplex structures that can be adopted by telomeric G-strand sequences.

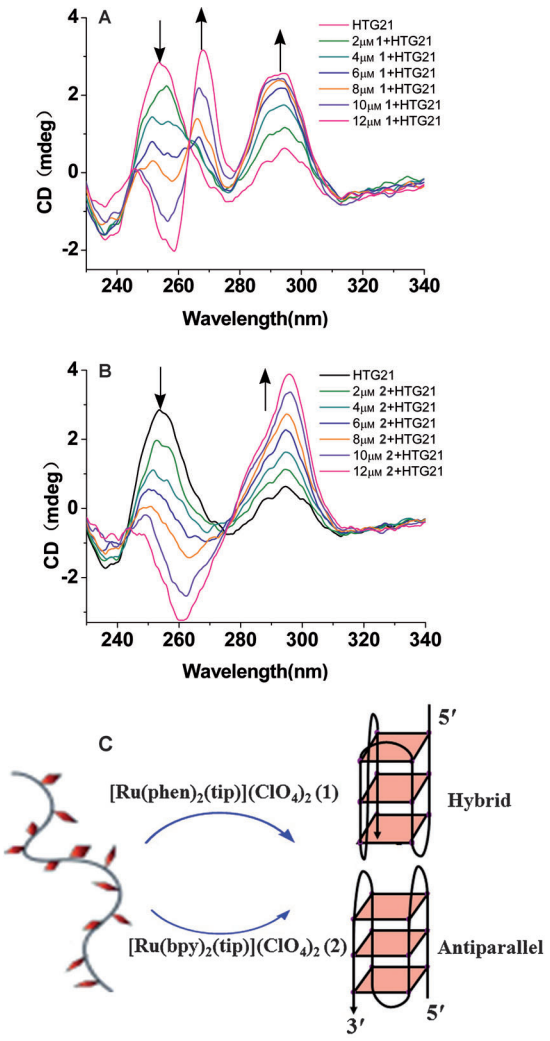

Figure 8. The CD titration spectra of HTG21 (2 μM) at increasing concentrations of complexes **1** (A) and **2** (B) in 10 mM Tris-HCl buffer, pH 7.40, 25 °C. Arrows indicate the increasing amounts of complexes. C) Representative illustration of the two Ru^{II} complexes inducing the single-stranded human telomeric DNA into different G-quadruplexes.

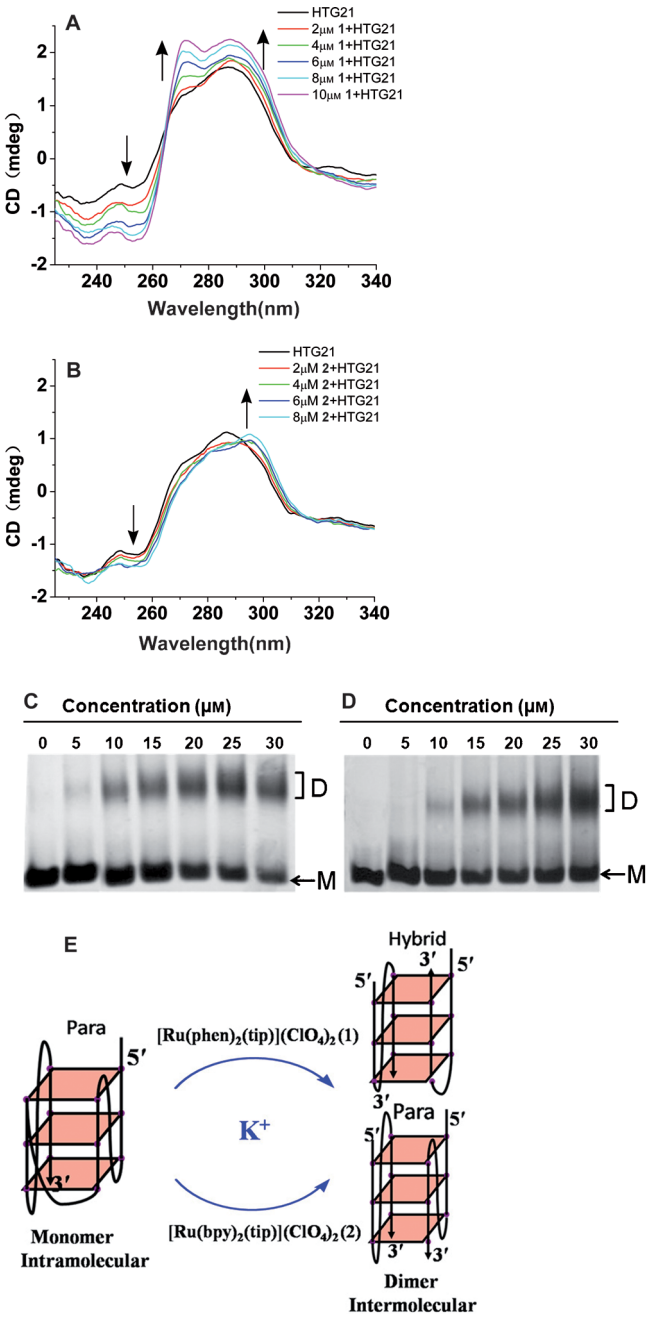

Figure 9. The CD titration spectra of HTG21 (2 μM) at increasing concentrations of complexes **1** (A) and **2** (B) in 10 mM Tris-HCl buffer, 100 mM KCl, pH 7.40, 25.0 °C. Arrows indicate the increasing amounts of complexes. Effects of complexes **1** (C) and **2** (D) on the assembly of the telo21 structure illustrated by PAGE analysis in 10 mM Tris-HCl (pH 7.40) containing 100 mM KCl. Major bands were identified as monomer (M) and dimer (D). E) Representative illustration of complexes converting the formation between the intra- and intermolecular structures in the presence of 100 mM KCl.

complex **1**, and a positive band at 270 nm started to appear. This result indicates that complex **1** can convert the parallel quadruplex into an obvious hybrid-type G-quadruplexes, thus signifying that this complex interacts more preferentially with the hybrid-type quadruplexes than does complex **2**. Both complexes could increase the intensity of the CD signals corresponding to HTG21 in a 100 mM solution of K^+, probably caused by the structural conversion between the intra- and intermolecular G-quadruplexes,[35] with reference to the following gel mobility shift assay (EMSA).

By contrast, the addition of increasing amounts of complexes **1** and **2** to HTG21 in 100 mM NaCl buffer resulted in no significant changes in the CD spectra (Figure S3). This result implies that the conformation of the G-quadruplex is stabilized by Na^+, and neither of the two Ru complexes could change the conformation of the G-quadruplex at high ionic strength.[36]

Specificity for G-quadruplex DNA by the electrophoretic mobility shift assay (EMSA)

The EMSA was performed to further identify whether the complexes can facilitate the formation of G-quadruplexes from the oligonucleotide HTG21 or converted the formation between the intra- and intermolecular structures. In the absence of Ru

complexes, only the band corresponding to the monomer could be observed in the electrophoretic mobility shift assays (Figure 9C,D), in accordance with the previous gel-shift data.[37] The increasing amounts of Ru complexes to HTG21 oligonucleotide resulted in the progressive appearance of new bands with reduced mobility, corresponding to the dimer forms. According to the quantification of the gels in the Figure S4, complex **1** gave the dimer band at 5 μM, whereas complex **2** did at a higher concentration (10 μM). In addition, complex 1 gave more of the dimer band (35%) at 30 μM than complex **2** (25%). These result reveal that both Ru complexes can efficiently promote different intermolecular quadruplex formation at high K^+ (Figure 9E), and complex **1** has a stronger quadruplex affinity and more preference for the hybrid-type quadruplex structure than complex **2**. This observation is in good agreement with the CD results in a solution of K^+ ions and the G-quadruplex stabilizing effects shown in other methods.

Stabilizing the G-quadruplex structure by the polymerase chain reaction (PCR)-stop assay

A PCR-stop assay was used to ascertain whether the Ru complexes could bind to a test oligomer HTG21 and therefore stabilize the G-quadruplex structure. The sequences of HTG21 and its corresponding complementary sequence (Rev 21G) can hybridize a final double-stranded DNA PCR product when used with Taq DNA polymerase as the catalyst. However, in the presence of some G-quadruplex stabilizers, the template sequence HTG21 was induced into a G-quadruplex structure that blocked the hybridization and the detection of the final PCR product. Figure 10 illustrates the inhibitory properties of the complexes

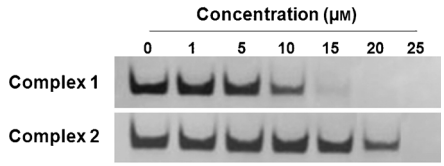

Figure 10. Effect of complexes **1** and **2** on the hybridization of HTG21 by the PCR-stop assay.

to a PCR process with similar concentration gradients. The inhibitory effect increased with increasing concentration. Complex **1** showed an inhibitory effect on telo21 at only 15 μM, whereas the effect of complex **2** was evident at 25 μM. The IC_{50} values (the concentrations that inhibited hybridization by 50%) of complexes **1** and **2** are 7.77 and 13.28 μM, respectively. A correlation between the PCR-stop assay results and FRET data could be drawn. Complexes with greater G-quadruplex structure-stabilizing power are generally better inhibitors of amplification in HTG21. Thus, complex **1** is a better G-quadruplex binder.

In vitro inhibition of the telomerase activity by the telomerase repeat amplification protocol (TRAP) assay

The TRAP assay is commonly used in evaluating telomerase activity in tissues or cell extracts and in determining the inhibitory properties of small molecules against telomerase.[38] The complexes exhibited high binding affinity and stabilizing ability to telomeric G-quadruplexes. Therefore, the telomerase inhibition of the complexes was investigated using the TRAP assay. In this experiment, solutions of complex **1** or **2** were added to the telomerase reaction mixture containing an extract from cracked $HepG_2$ cell lines. The results of the telomerase activity are listed in Figure 11. At a concentration of 5–10 μM for complex **1**, the TRAP assay revealed a dose-dependent inhibition of the telomere, and the number of bands clearly decreased with respect to the control. By contrast, no complete inhibition was observed in the presence of complex **2**, even at 12.5 μM concentration. Complex **1** ($^{Tel}IC_{50} = 5.8$ μM) exhibited a better inhibitory effect on the telomerase activity compared with complex **2** ($^{Tel}IC_{50} > 12.5$ μM). This result not only agrees with the experimental data from the aforementioned studies, but also indicates that complex **1** might be a potential human telomerase inhibitor.

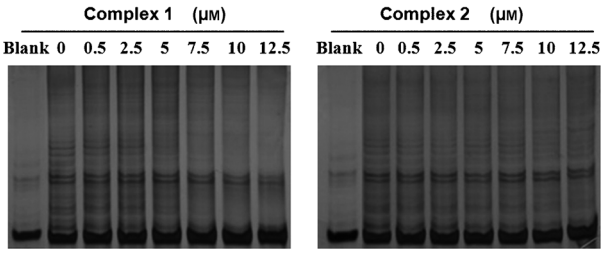

Figure 11. The influence of complexes **1** and **2** to the telomere activity of HepG2.

Cytotoxicity test by the 3-(4,5-dimethylthiazol-2-yl)-2, 5-diphenyltetrazolium bromide (MTT) assay

The cytotoxicity of the Ru complexes against $HepG_2$, SW620, A549, MDA-MB-231, and NIH/3T3 cell lines were determined by the MTT assay. Details of the results are given in Table 3 and Figure 12. Complexes exhibited a differential cytotoxicity

Table 3. Cytotoxic effects of Ru complexes and Cisplatin on human cancer cell lines.

Complex	IC_{50} values [μM][a]				
	$HepG_2$	SW620	A549	MDA-MB-231	NIH/3T3
1	11.21 ± 2.02	27.43 ± 3.23	25.56 ± 3.52	19.90 ± 1.42	> 100
2	15.56 ± 2.83	54.38 ± 2.26	34.34 ± 3.74	40.37 ± 1.21	59.31 ± 2.36
Cisplatin	13.61 ± 1.13	30.02 ± 1.81	3.23 ± 0.27	–	19.72 ± 1.59

[a] The values are expressed as the mean ± standard deviation (triplicates).

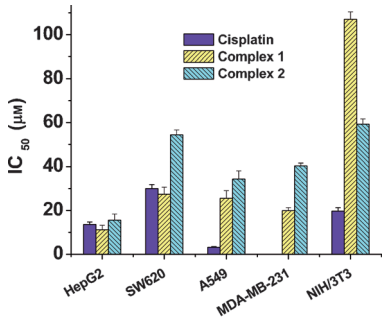

Figure 12. IC_{50} values of Ru complexes and Cisplatin on human cancer cell lines.

against cancer cells after 2 days. In particular, we found the IC_{50} values of the Ru complexes on NIH/3T3 from 59.31 μM to greater 100 μM were significantly higher than those of Cisplatin (19.72 μM). This finding suggests that this series of complexes inhibited the growth of cancer cell lines better than normal cells and the Ru^{II} complexes were much less toxic toward normal cells. Complex **1** exhibited a broad spectrum of inhibition on human cancer cells, with IC_{50} values ranging from 11.21 to 27.43 μM. More importantly, as evidenced by the lower IC_{50} values, complex **1** exhibited much higher antiproliferative activities on the cancer cell lines than complex **2**. Notably, complex **1** showed a distinct preference for the HepG2 cells (IC_{50} = 11.21 μM, lower than Cisplatin in killing HepG2 cells).This result, combined with the TRAP assay, suggests that the cytotoxicity of this metal complex may be attributed to its role in telomerase inhibition.

Conclusion

Two Ru^{II} polypyridyl complexes as telomeric quadruplex stabilizers have been synthesized and evaluated using biophysical and biochemical studies. The CD data reveal that complex **1** selectively induces the formation of hybrid-type quadruplexes, whereas complex **2** could induce antiparallel G-quadruplexes in the absence of any salt and keep parallel G-quadruplexes in a solution of K^+ ions. Absorption and emission studies suggest that complex **1** can bind to the G-quadruplex with larger binding constants. The FRET and thermal denaturation studies imply that complex **1**, increasing the ΔT_m value by 18.8 °C at 2 μM, is a more effective quadruplex-DNA stabilizer. In addition, continuous variation analyses, NMR spectroscopy, and molecular modeling were used to investigate the multiple interaction (mainly intercalating) of complex **1** at the 3′-terminal face through a 1:1 [quadruplex]/[complex] binding mode ratio. The biochemical studies, including the PCR-stop and EMSA assays, further demonstrate that both complexes can promote HTG21 into the dimer forms. Complex **1** inhibits the telomerase activity in a cell-free system by the TRAP assay. The MTT assay determines that complex **1** is moderately cytotoxic (IC_{50} = 11.21 μM) in the $HepG_2$ cell lines.

Hence, complex **1** containing a larger planar ancillary ligand such as 1,10-phenanthroline, which can interact with grooves/loops and the phosphate backbone of quadruplexes, is a better telomeric quadruplex stabilizer and telomerase inhibitor than complex **2**. These notable differences in the two complexes prove that planarity and π-delocalized system are vital for the G-quadruplex recognition in binding. Furthermore, complex **1** exhibits an antitumor function by locking a telomeric DNA into a G-quadruplex conformation that cannot be extended by telomerase. Ruthenium complexes definitely represent an exciting new strategy in designing new antitumor agents for targeting DNA quadruplexes.

Experimental Section

CAUTION! Metal perchlorates are potentially explosive and should therefore be handled with great care.

Reagents and materials

The oligomers or primers used in this study were purchased from Sangon (Shanghai, China) and used without further purification. The DNA oligomers include HTG21 = 5′-$G_3(T_2AG_3)_3$-3′, G4A3 = 5′-TAGGGTTA-3′, double-stranded competitor (ds26 = 5′-CAATCG-GATCGAATTCGATCCGATTG-3′, and F21T = 5′-FAM-d($G_3[T_2AG_3]_3$)-TAMRA-3′, of which the donor fluorophore FAM is 6-carboxy-fluorescein and the acceptor fluorophore TAMRA is 6-carboxytetramethylrhodamine. Concentrations of these oligomers were determined by measuring the absorbance at 260 nm after melting. Single-strand extinction coefficients were calculated from mononucleotide data using a nearest-neighbor approximation.[39] The formations of intramolecular G-quadruplexes were carried out as follows: the oligonucleotide samples were annealed in different buffers at 95 °C for 5 min, slowly cooled to RT, and then incubated at 4 °C for 12 h. Buffer A: 10 mM tris(hydroxymethyl)aminomethane-HCl (Tris-HCl), pH 7.40; buffer B: 10 mM Tris-HCl, 100 mM NaCl, pH 7.40; buffer C: 10 mM Tris-HCl, 100 mM KCl, pH 7.40. Other reagents and solvents were purchased commercial sources unless otherwise specified. Doubly distilled water was used to prepare buffer solutions.

Physical measurement

Electrospray ionization mass spectra (ESI-MS) were acquired by using a Thermo Finnigan LCQ DECA XP ion-trap mass spectrometer, equipped with an ESI source. The ^1H NMR spectra were acquired on a Varian 400 MHz spectrometer with $(CD_3)_2SO$ as solvent at RT, and all chemical shift values were given relative to tetramethylsilane (TMS). Elemental analyses for C, H, and N were carried out with a PerkinElmer 240 °C elemental analyzer and purity of all target compounds used in the biophysical and biological studies was > 95 %. The absorption spectra in the UV/Vis region were recorded on a Varian Cary 300 spectrophotometer. Emission spectra of the synthetic Ru complexes were measured on a Shimadzu RF-5000 fluorescence spectrophotometer with excitation at 468 nm. The CD spectra were measured on a JASCO J-810 spectropolarimeter and high-frequency noise was filtered out using JASCO J-600 software.

Synthesis and characterization

1,10-phenanthroline-5,6-dione, $[Ru(phen)_2Cl_2]\cdot 2H_2O$, and $[Ru(bpy)_2Cl_2]\cdot 2H_2O$ were prepared and characterized according to the literature.[40]

Synthesis of 2-thiophenimidazo[4,5-*f*][1,10]phenanthroline (TIP)

The ligand was prepared by using modified literature procedures.[41] A mixture of 1,10-phenanthroline-5,6-dione (0.21 g, 1 mmol), 2-thiophene-carboxaldehyde (0.14 g, 1.2 mmol), ammonium acetate (0.15 g, 20 mmol), and glacial acetic acid (20 mL) was heated at reflux for 4 h. The cooled deep-red solution was diluted with water (40 mL) and neutralized with ammonium hydroxide to give a yellow precipitate. The precipitate was collected and purified by column chromatography on silica gel (60–100 mesh) with ethanol as eluent to give the ligand as yellow powder (yield of 0.25 g, 85%). ESI-MS (MeOH) *m/z*: 302.0 (100, $[M+H]^+$); elemental analysis (%) calcd for $C_{17}H_{10}N_4S$: C 67.53, H 3.33, N 18.53; found: C 67.52, H 3.41, N 18.60.

Synthesis of $[Ru(phen)_2(TIP)](ClO_4)_2$ (1)

Complex **1** was synthesized by using a modified literature procedure.[42] $[Ru(phen)_2Cl_2]\cdot 2H_2O$ (0.29 g, 0.5 mmol) was dissolved in glacial acetic acid (20 mL) and **tip** (0.18 g, 0.6 mmol) was added. The mixture was heated at reflux for 8 h under argon. Upon cooling, a red precipitate was obtained by dropwise addition of saturated aqueous $NaClO_4$ solution. The precipitated complex was isolated by filtration and air-dried, then purified by chromatography on alumina (200 mesh) with acetonitrile (ACN)/toluene (4:1, v/v) as an eluent to give the complex as red (yield of 0.27 g, 56%). The sample shows good solubility in solvents such as ACN, dimethyl sulfoxide (DMSO), and acetone. ^{1}H NMR ([D$_6$]DMSO): $\delta = 8.94$ (d, 2H), 8.76 (d, 4H), 8.39 (s, 4H), 8.10–8.12 (m, 4H), 7.89 (d, 3H), 7.75–7.79 (m, 4H), 7.70 (t, 2H), 7.65 (d, 1H), 7.24 ppm (t, 1H); UV/Vis (ACN; λ (ε)): 457 (32400), 288 (84700), 262 nm (149500 $M^{-1}cm^{-1}$); ESI-MS (ACN) *m/z*: 864.9 ($[M-ClO_4]^+$), 763.2 ($[M-2ClO_4-H]^+$), 382.3 ($[M-2ClO_4]^{2+}$); elemental analysis (%) calcd for $C_{41}H_{26}N_8Cl_2O_8RuS$: C 51.15, H 2.72, N 11.64; found: C 51.13, H 2.81, N 11.56. See NMR and ESI-MS spectra in the Supporting Information.

Synthesis of $[Ru(bpy)_2(TIP)](ClO_4)_2$ (2)

Complex **2** was prepared by the same method as above but with $[Ru(bpy)_2Cl_2]\cdot 2H_2O$ (0.242 g, 0.5 mmol) to give a yield of 0.228 g, 50%. ^{1}H NMR ([D$_6$]DMSO): $\delta = 8.98$ (d, 2H), 8.87 (d, 2H), 8.83 (d, 2H), 8.22 (t, 2H), 8.11 (t, 2H), 7.93 (d, 2H), 7.82–7.87 (m, 5H), 7.64 (d, 1H), 7.59 (t, 4H), 7.37 (t, 2H), 7.24 ppm (t, 1H); UV/Vis (ACN; λ (ε)): 462 (17100), 286 (66800), 244 nm (40500 $M^{-1}cm^{-1}$); ESI-MS (ACN): *m/z* = 814.7 ($[M-ClO_4]^+$), 715.1 ($[M-2ClO_4-H]^+$), 358.3 ($[M-2ClO_4]^{2+}$); elemental analysis (%) calcd for $C_{37}H_{26}N_8Cl_2O_8RuS$: C 48.58, H 2.87, N 12.25; found: C 48.62, H 2.77, N 12.18. See NMR and ESI-MS spectra in the Supporting Information.

Absorption and emission spectra

Analysis of absorption and emission spectra are the most common ways to investigate the interactions of complexes with DNA. The titration was performed by using a fixed complex concentration (5 μM in buffer C) to which increments of the DNA stock solution were added at RT. The volume of the complex was 3000 μL. Solutions of complex DNA were incubated for 5 min before absorption spectra were recorded. The titration processes were repeated several times until no change was observed in the spectra, indicating that binding saturation was achieved. Changes in the concentration of metal complexes as a result of dilution at the end of each titration were negligible. The titrations for each sample were repeated at least three times.

Continuous variation analysis

Continuous variation analysis was performed by using a Shimadzu RF-5000 fluorescence spectrophotometer following previously published procedures.[25] Each complex and HTG21 were prepared as 10 μM solution in Tris-HCl buffer containing 100 mM KCl. Two series of solutions were used for the experiments: one with varying mole fractions of complex and HTG21, and another one with varying concentrations of complex. The sum of the complex and HTG21 concentrations was always 10 μM. Their emission spectrum was collected from 500 to 750 nm using a quartz cell with a path length of 1 cm at 25 °C. The ΔI values were calculated by subtracting the fluorescence intensity of complex solution without HTG21 from the fluorescence intensity of corresponding complex solution with HTG21 at λ_{max}. This value was plotted versus the complex mole fraction to generate a Job plot. Binding stoichiometries were obtained from the intercepts of the linear plot obtained by linear least-squares fits to the left- and right-hand portions of the Job plots. Final analysis of the data was carried out using Origin 7.5 software (Origin Lab Corp.).

Thermal denaturation study

The thermal denaturation study was carried by using a JASCO J-810 spectropolarimeter equipped with a Peltier temperature-controlling programmer PTP-6. With the use of the thermal melting program, the temperature of the cell containing the cuvette was ramped from 40 to 100 °C. Thermal melting curves and calculation of ΔT_m values were performed in Tris-KCl buffer with 2 μM HTG21 in the presence or absence of 20 μM Ru complexes. The CD spectrum at 295 nm was monitored at a rate of 1 °C min^{-1}, and measured every 1 °C.

FRET assay

The fluorescent-labeled oligonucleotide F21T, was prepared as a 100 μM solution in buffer C and then annealed by heating to 90 °C for 5 min, and subsequently cooled to RT overnight. Fluorescence melting curves were determined by using a Bio-Rad iQ5 real-time PCR detection system, using a total reaction volume of 20 μL, with 0.2 μM of labeled oligonucleotide and different concentrations of complexes. Fluorescence readings with excitation at 470 nm and detection at 530 nm were taken at intervals of 1 °C over the range 37–99 °C, with a constant temperature being maintained for 30 s prior to each reading to ensure a stable value. The melting of the G-quadruplex was monitored alone or in the presence of various concentrations of complexes and/or of double-stranded competitor ds26. Final analysis of the data was carried out using Origin 7.5 software (Origin Lab Corp.).

NMR experiments

The ^{1}H NMR experiments were performed by using a Bruker AVANCE 400 spectrometer with a typical acquisition condition of 45 pulse length, 2.0 s relaxation delay, 16 K data points, 16–32 transients. The stock solutions of G4A3 G-quadruplex were prepared by dissolving the sample in 90% H_2O/10% D_2O with 150 mM KCl, 25 mM KH_2PO_4, and 1 mM ethylenediaminetetraacetic acid (EDTA), pH 7.4. Aliquots of stock solutions containing complex were titrat-

ed directly into the DNA solution inside an NMR tube. The ^{1}H NMR spectra were recorded at 300 K by the pulse program with gradients for water suppression.

Molecular docking calculations

A model study on the interaction between complex **1** and G-quadruplex DNA was performed by using Accelrys Discovery Studio 2.1 Software. The CHARMm force-field was used in the input of the calculations. The correction of the partial charge distribution for all atoms in the Ru^{II} complexes was made following the output from Gaussian 03.[43] Model building and optimization were performed using the model building and energy-minimization modules of the Accelrys Software Package. The DNA crystal structures for $d(T_2AG_3T)_4$ (PDB code 1NP9)[44] was downloaded from the Protein Data Bank. The docking options were then performed to find the most stable and favorable orientation. The binding site was assigned across the all of the minor and major grooves of the DNA molecule. Interaction energies of Ru–DNA complexes can be estimated by calculating the difference between their total energies and the sum of lowest energies found for the optimized structures of free DNA and binuclear complex. The negative of the interaction energy is the binding energy, ΔE=TE−sum of the individual energy (BE), where ΔE is the interaction energy, TE is the total energy of DNA/complex, and BE is the binding energy.[45]

Circular dichroism study

All CD experiments were measured at RT using a quartz cell with a path length of 1 cm. The spectra were collected from 220 to 400 nm and with a scanning speed of 200 nm min^{-1}. The bandwidth was 5 nm, and the response time was 2 s. The CD titration was performed at a fixed HTG21 concentration (2 μM) with various concentrations (0–5 mol equiv) of the complexes in different buffers; (a) 10 mM Tris-HCl, pH 7.4; (b) 100 mM NaCl, 10 mM Tris-HCl, pH 7.4; (c) 100 mM KCl,10 mM Tris-HCl, pH 7.4. After each addition of Ru complex, the reaction was stirred and allowed to equilibrate for at least 5 min (until no elliptic changes were observed) and a CD spectrum were measured. During the experiment, the instrument was flushed continuously with pure nitrogen.

Polymerase chain reaction (PCR)-stop assay

The PCR-stop assay was carried out according to a modified protocol of a previous study.[46] The test oligomers HTG21 and the corresponding complementary sequences Rev 21 G ($ATCGCT_2CTCGTC_3TA_2C_2$) were used in the current study. The reactions were performed in 1×PCR buffer, containing 10 pmol of each oligonucleotide, 0.16 mM dNTP, 2.5 U Taq polymerase, and different concentrations of complexes. Reaction mixtures were incubated in a thermocycler with the following cycling conditions: 94 °C for 3 min, followed by 30 cycles of 94 °C for 30 s, 58 °C for 30 s, and 72 °C for 30 s. The products generated from PCR were then analyzed on 15% nondenaturing polyacrylamide gels in 1×TBE and silver stained. The photos were taken and IC_{50} values were calculated.

Gel mobility shift assay

The formation of G-quadruplex DNA was carried out as described in the literature.[47] Briefly,10 μM the oligomer (HTG21) was heated at 95 °C for 10 min in 10 mM Tris-HCl (pH 7.40) containing 100 mM KCl. After the DNA was cooled to RT, a 10 μL stock solution of metal complex was added to each sample to produce the specified concentrations at a total volume of 20 μL. The reaction mixture was incubated for 12 h at RT. Each mixture was added 4 μL of loading buffer (50% glycerol, 0.25% bromophenol blue, and 0.25% xylene cyanol) and analyzed on a 20% native polyacrylamide gel electrophoresis (PAGE; the gel was pre run for 30 min). Electrophoresis proceeded for 2 h in TBE (Tris-borate EDTA) running buffer. The gels were silver-stained according to a previously reported protocol.[47]

TRAP assay

The TRAP assay was carried out according to a modified protocol of a previous study.[48] Telomerase extraction from $HepG_2$ cells. The TRAP assay was performed in two steps: 1) telomerase-mediated extension of the forward primer (TS: 5′-AATCCGTCGAGCAGAGTT-3′) contained in a 20 μL reaction mixture comprising TRAP buffer (20 mM, pH 8.3), 68 mM KCl, 1.5 mM $MgCl_2$, 1 mM EGTA, 0.05% v/v Tween-20, 0.05 μg of bovine serum albumin, 50 μM of each deoxynucleotide triphosphate, 0.1 μg of TS primer, and 3 μCi of [R-32P]dCTP. The protein (0.04 μg) was incubated with the reaction mixture ±agent (acid addition and quaternary dimethiodide salts) at final concentrations of up to 50 μM for 20 min at 25 °C. Analysis buffer (no protein) control, heat-inactivated protein control, and 50% protein (0.02 μg) control were included in each assay. 2) While the mixture was being heated at 80 °C in a polymerase chain reaction (PCR) block of a thermal cycler for 5 min to inactivate telomerase activity, 0.1 μg of reverse CX primer (3′-AATCCCATTCCCATTCCCATTCCC-5′) and two units of Taq DNA polymerase were added. A three-step PCR was then performed: 94 °C for 30 s, 50 °C for 30 s, and 72 °C for 1 min for 31 cycles. Telomerase-extended PCR products in the presence or absence of complexes were determined by electrophoretic separation using 8% w/w acrylamide denaturing gels.

MTT assay

$HepG_2$, SW620, A549, MDA-MB-231, and NIH/3T3 were seeded on 96-well plates (1.0×10^3 per well) and exposed to various concentrations of complexes. The microplate was incubated for 48 h at 37 °C, 5% CO_2, and 95% air in a humidified incubator. After incubation, 10 μL of MTT reagent (5 mg mL^{-1}) was added to each well and further incubated for 2 h. The cells in each well were then treated with DMSO (150 μL for each well) and the optical density (OD) was recorded at 570 nm. All drug doses were parallel tested in triplicate, and the IC_{50} values were derived from the mean OD values of the triplicate tests versus drug concentration curves.[49]

Acknowledgements

This study was supported by the National Natural Science Foundation of China (20871056, 21171070), the Planned Item of Science and Technology of Guangdong Province (c1011220800060), the Fundamental Research Funds for the Central Universities, the Planned Item of Science, and the Fundamental Research Foundation of Shenzhen City (Major Project; JC201005250058A).

Keywords: antitumor agents · bioinorganic chemistry · DNA · G-quadruplex DNA · ruthenium complexes · telomerase

[1] a) J. T. Davis, *Angew. Chem.* **2004**, *116*, 684 – 716; *Angew. Chem. Int. Ed.* **2004**, *43*, 668 – 698; b) J. L. Huppert, *Chem. Soc. Rev.* **2008**, *37*, 1375 – 1384; c) J. T. Wang, Y. Li, J. H. Tan, L. N. Ji, Z. W. Mao, *Dalton Trans.* **2011**, *40*, 564 – 566.
[2] a) D. Monchaud, M. P. Teulade-Fichou, *Org. Biomol. Chem.* **2008**, *6*, 627 – 636; b) S. Burge, G. N. Parkinson, P. Hazel, A. K. Todd, S. Neidle, *Nucleic Acids Res.* **2006**, *34*, 5402.
[3] E. H. Blackburn, *Nature* **1991**, *350*, 569 – 573.
[4] a) C. B. Harley, A. B. Futcher, C. W. Greider, *Nature* **1990**, *345*, 458 – 460; b) M. Y. Kim, H. Vankayalapati, K. Shin-ya, K. Wierzba, L. H. Hurley, *J. Am. Chem. Soc.* **2002**, *124*, 2098 – 2099.
[5] L. R. Kelland, *Anti-Cancer Drugs* **2000**, *11*, 503 – 513.
[6] N. W. Kim, M. A. Piatyszek, K. R. Prowse, C. B. Harley, M. D. West, P. L. Ho, G. M. Coviello, W. E. Wright, S. L. Weinrich, J. W. Shay, *Science* **1994**, *266*, 2011 – 2015.
[7] a) C. I. Nugent, V. Lundblad, *Genes Dev.* **1998**, *12*, 1073 – 1085; b) A. De Cian, L. Lacroix, C. Douarre, N. Temime-Smaali, C. Trentesaux, J. F. Riou, J. L. Mergny, *Biochimie* **2008**, *90*, 131 – 155.
[8] a) T. Ou, Y. Lu, J. Tan, Z. Huang, K. Y. Wong, L. Gu, *ChemMedChem* **2008**, *3*, 690 – 713; b) J. L. Zhou, Y. J. Lu, T. M. Ou, J. M. Zhou, Z. S. Huang, X. F. Zhu, C. J. Du, X. Z. Bu, L. Ma, L. Q. Gu, *J. Med. Chem.* **2005**, *48*, 7315 – 7321; c) E. M. Rezler, J. Seenisamy, S. Bashyam, M. Y. Kim, E. White, W. D. Wilson, L. H. Hurley, *J. Am. Chem. Soc.* **2005**, *127*, 9439 – 9447.
[9] a) S. T. D. Hsu, P. Varnai, A. Bugaut, A. P. Reszka, S. Neidle, S. Balasubramanian, *J. Am. Chem. Soc.* **2009**, *131*, 13399 – 13409; b) B. Rubis, M. Kaczmarek, N. Szymanowska, E. Galezowska, A. Czyrski, B. Juskowiak, T. Hermann, M. Rybczynska, *Invest. New Drugs* **2009**, *27*, 289 – 296.
[10] K. L. Haas, K. J. Franz, *Chem. Rev.* **2009**, *109*, 4921 – 4960.
[11] a) R. T. Wheelhouse, D. Sun, H. Han, F. X. Han, L. H. Hurley, *J. Am. Chem. Soc.* **1998**, *120*, 3261 – 3262; b) F. Gao, H. Chao, L. N. Ji, *Chem. Biodiversity* **2008**, *5*, 1962 – 1979.
[12] L. Xu, G. L. Liao, X. Chen, C. Y. Zhao, H. Chao, L. N. Ji, *Inorg. Chem. Commun.* **2010**, *13*, 1050 – 1053.
[13] J. E. Reed, A. A. Arnal, S. Neidle, R. Vilar, *J. Am. Chem. Soc.* **2006**, *128*, 5992 – 5993.
[14] S. Shi, X. Geng, J. Zhao, T. Yao, C. Wang, D. Yang, L. Zheng, L. Ji, *Biochimie* **2010**, *92*, 370 – 377.
[15] S. Shi, J. Liu, T. Yao, X. Geng, L. Jiang, Q. Yang, L. Cheng, L. Ji, *Inorg. Chem.* **2008**, *47*, 2910 – 2912.
[16] T. Wilson, M. P. Williamson, J. A. Thomas, *Org. Biomol. Chem.* **2010**, *8*, 2617 – 2621.
[17] A. Ghosh, P. Das, M. R. Gill, P. Kar, M. G. Walker, J. A. Thomas, A. Das, *Chem. Eur. J.* **2011**, *17*, 2089 – 2098.
[18] L. Xu, D. Zhang, J. Huang, M. Deng, M. Zhang, X. Zhou, *Chem. Commun.* **2010**, *46*, 743 – 745.
[19] C. Rajput, R. Rutkaite, L. Swanson, I. Haq, J. A. Thomas, *Chem. Eur. J.* **2006**, *12*, 4611 – 4619.
[20] C. Wei, G. Jia, J. Yuan, Z. Feng, C. Li, *Biochemistry* **2006**, *45*, 6681 – 6691.
[21] J. Sun, Y. An, L. Zhang, H. Y. Chen, Y. Han, Y. J. Wang, Z. W. Mao, L. N. Ji, *J. Inorg. Biochem.* **2011**, *105*, 149 – 154.
[22] S. Satyanarayana, J. C. Dabrowiak, J. B. Chaires, *Biochemistry* **1992**, *31*, 9319 – 9324.
[23] I. Haq, J. O. Trent, B. Z. Chowdhry, T. C. Jenkins, *J. Am. Chem. Soc.* **1999**, *121*, 1768 – 1779.
[24] a) M. R. Gill, J. A. Thomas, *Chem. Soc. Rev.*, **2012**, *41*, 3179 – 3192; b) Y. Li, Z. Y. Yang, J. C. Wu, *Eur. J. Med. Chem.* **2010**, *45*, 5692 – 5701; c) S. N. Georgiades, N. H. Abd Karim, K. Suntharalingam, R. Vilar, *Angew. Chem.* **2010**, *122*, 4114 – 4128; *Angew. Chem. Int. Ed.* **2010**, *49*, 4020 – 4034.
[25] J. Dash, Z. A. E. Waller, G. D. Panto, S. Balasubramanian, *Chem. Eur. J.* **2011**, *17*, 4571 – 4581.
[26] A. D. Moorhouse, A. M. Santos, M. Gunaratnam, M. Moore, S. Neidle, J. E. Moses, *J. Am. Chem. Soc.* **2006**, *128*, 15972 – 15973.
[27] J. L. Mergny, L. Lacroix, M. P. Teulade-Fichou, C. Hounsou, L. Guittat, M. Hoarau, P. B. Arimondo, J. P. Vigneron, J. M. Lehn, J. F. Riou, *Proc. Natl. Acad. Sci. USA* **2001**, *98*, 3062 – 3067.
[28] D. L. Ma, C. M. Che, S. C. Yan, *J. Am. Chem. Soc.* **2008**, *130*, 1835 – 1846.
[29] E. Gavathiotis, R. A. Heald, M. F. G. Stevens, M. S. Searle, *Angew. Chem.* **2001**, *113*, 4885 – 4887; *Angew. Chem. Int. Ed.* **2001**, *40*, 4749 – 4751.
[30] A. T. Phan, V. Kuryavyi, H. Y. Gaw, D. J. Patel, *Nat. Chem. Biol.* **2005**, *1*, 167 – 173.
[31] P. Murat, Y. Singh, E. Defrancq, *Chem. Soc. Rev.*, **2011**, *40*, 5293 – 5307.
[32] W. Peti, J. Meiler, R. Brüschweiler, C. Griesinger, *J. Am. Chem. Soc.* **2002**, *124*, 5822 – 5833.
[33] R. Jin, B. L. Gaffney, C. Wang, R. A. Jones, K. J. Breslauer, *Proc. Natl. Acad. Sci. USA* **1992**, *89*, 8832 – 8836.
[34] V. Dapic, V. Abdomerovi, R. Marrington, J. Peberdy, A. Rodger, J. O. Trent, P. J. Bates, *Nucleic Acids Res.* **2003**, *31*, 2097 – 2107.
[35] C. T. Lin, T. Y. Tseng, Z. F. Wang, T. C. Chang, *J. Phys. Chem. B.* **2011**, *115*, 2360 – 2370.
[36] A. Ambrus, D. Chen, J. Dai, T. Bialis, R. A. Jones, D. Yang, *Nucleic Acids Res.* **2006**, *34*, 2723 – 2735.
[37] H. Han, D. R. Langley, A. Rangan, L. H. Hurley, *J. Am. Chem. Soc.* **2001**, *123*, 8902 – 8913.
[38] D. Gomez, J. L. Mergny, J. F. Riou, *Cancer Res.* **2002**, *62*, 3365 – 3368.
[39] M. E. Reichmann, S. A. Rice, C. A. Thomas, P. Doty, *J. Am. Chem. Soc.* **1954**, *76*, 3047 – 3053.
[40] S. Shi, J. Liu, J. Li, K. C. Zheng, X. M. Huang, C. P. Tan, L. M. Chen, L. N. Ji, *J. Inorg. Biochem.* **2006**, *100*, 385 – 395.
[41] J. Liu, W. Zheng, S. Shi, C. Tan, J. Chen, K. Zheng, L. Ji, *J. Inorg. Biochem.* **2008**, *102*, 193 – 202.
[42] W. J. Mei, J. Liu, K. C. Zheng, L. J. Lin, H. Chao, A. X. Li, F. C. Yun, L. N. Ji, *Dalton Trans.* **2003**, 1352 – 1359.
[43] A. K. Patra, T. Bhowmick, S. Roy, S. Ramakumar, A. R. Chakravarty, *Inorg. Chem.* **2009**, *48*, 2932 – 2943.
[44] E. Gavathiotis, M. S. Searle, *Org. Biomol. Chem.* **2003**, *1*, 1650 – 1656.
[45] R. Bhowmik, K. S. Katti, D. Katti, *Polymer* **2007**, *48*, 664 – 674.
[46] B. Fu, D. Zhang, X. Weng, M. Zhang, H. Ma, Y. Ma, X. Zhou, *Chem. Eur. J.* **2008**, *14*, 9431 – 9441.
[47] a) J. L. Zhou, Y. J. Lu, T. M. Ou, J. M. Zhou, Z. S. Huang, X. F. Zhu, C. J. Du, X. Z. Bu, L. Ma, L. Q. Gu, *J. Med. Chem.* **2005**, *48*, 7315 – 7321; b) D. Sun, R. Zhang, F. Yuan, D. Liu, Y. Zhou, J. Liu, *Dalton Trans.*, **2012**, *41*, 1734 – 1741.
[48] a) H. L. Huang, Y. J. Liu, C. H. Zeng, J. H. Yao, Z. H. Liang, Z. Z. Li, F. H. Wu, *J. Mol. Struct.* **2010**, *966*, 136 – 143; b) D. Sun, Y. N. Liu, D. Liu, R. Zhang, X. Yang, J. Liu, *Chem. Eur. J.* **2012**, *18*, 4285 – 4295.
[49] Y. Ma, T. M. Ou, J. H. Tan, J. Q. Hou, S. L. Huang, L. Q. Gu, Z. S. Huang, *Eur. J. Med. Chem.* **2011**, *46*, 1906 – 1913.

Received: February 29, 2012
Revised: April 17, 2012
Published online on May 21, 2012

